BIS ENERGY AND ENGINEERING

Volume 3 2026 | DOI: 10.31603/biseeng.572
7th Borobudur International Symposium on Science and Technology (BIS-STE) 2025

UNIMMA PRESS
Universitas Muhammadiyah Magelang

Effect of SMAW heat input variations on the microstructure and mechanical properties of SS400 low-carbon steel

Ruspita Sihombing*[1], Hasan Basri[1], Muhammad Ardi[1], and Swarto[1]

[1] Mechanical Engineering Department, Politeknik Negeri Samarinda, Indonesia
*Corresponding author email: ruspita@polnes.ac.id

Abstract

This study aims to analyze the effect of heat input variation in the Shielded Metal Arc Welding (SMAW) process on the microstructure and mechanical properties of SS400 low-carbon steel. The heat input variations used in this research were 1.24 kJ/mm, 1.84 kJ/mm, and 2.20 kJ/mm. The conducted tests included microstructural analysis using metallographic techniques and tensile testing to determine the relationship between welding parameters and material characteristics. The results show that heat input variation significantly influences changes in ferrite and pearlite phases with a 95% confidence level. At the lowest heat input of 1.24 kJ/mm, fine ferrite grains and uniformly distributed pearlite were formed, resulting in the highest mechanical performance, with a tensile strength of 466.11 MPa and a yield strength of 345.89 MPa. Increasing the heat input to 1.84 kJ/mm and 2.20 kJ/mm caused grain coarsening and a reduction in pearlite fraction, which led to a decrease in tensile strength by approximately 0.08– 0.10% and a decline in yield strength by 16.7–41.39%. These conditions caused the material to become softer and more susceptible to plastic deformation. Based on the findings, the optimal heat input to achieve the best joint strength for SS400 steel using the SMAW process is 1.24 kJ/mm. This study provides important insights for optimizing welding parameters to improve the strength and reliability of welded joints in construction and manufacturing applications.

Keywords

Head input, SMAW, SS400 steel, Microstructure, Tensile strength, Yield strength

Published:
May 04, 2026

This work is licensed under a Creative Commons Attribution-NonCommercial 4.0 International License

Selection and Peer-review under the responsibility of the 7th BIS-STE 2025 Committee

Introduction

Welding is a widely applied metal-joining technique in manufacturing and construction sectors due to its ability to create permanent joints with high efficiency. Among the various welding techniques available, Shielded Metal Arc Welding (SMAW) is one of the most extensively used because of its versatility, ease of operation, and relatively low cost. However, the quality of a welded joint strongly depends on the process parameters, particularly the amount of heat input applied during welding. Heat input

plays a crucial role in determining the resulting microstructure and mechanical properties of the weld. Insufficient heat input may lead to poor penetration and porosity, whereas excessive heat input can cause grain growth, the formation of undesirable phases, and a deterioration in mechanical strength. Therefore, controlling heat input is essential for achieving an optimal balance between strength, toughness, and reliability in welded joints.

Low-carbon steel such as SS400 is widely used in construction, automotive, and fabrication industries due to its favorable combination of ductility, weldability, and cost-effectiveness. However, microstructural changes caused by varying thermal cycles during welding can significantly affect joint performance. A comprehensive understanding of the influence of heat input on microstructural evolution particularly in the weld metal and the Heat Affected Zone (HAZ) is essential to ensure joint quality in structural applications.

Considering these factors, this study was conducted to analyze the effects of heat input variation in the SMAW process on the microstructural changes, tensile strength, and yield strength of SS400 low-carbon steel. The primary objective of this research is to determine the optimum heat input that provides the best combination of strength and toughness, while also offering scientific guidance for more efficient and reliable parameter control in industrial welding applications.

Previous research findings

Low-carbon steel type SS400 is widely used in construction, machinery, and fabrication industries due to its good weldability, adequate tensile strength, and relatively low cost (Qi et al. 2024) (Muthusamy et al. 2016). However, the welding process may significantly alter the mechanical properties and microstructure of the material due to the thermal effects generated during welding (Xia and Kou 2021) (Saad et al. 2025). One of the key factors that strongly influences weld quality is heat input, which represents the amount of thermal energy supplied per unit length of weld (Awad et al. 2025) (Ajenifuja, Popoola, and Popoola 2025).

In the Shielded Metal Arc Welding (SMAW) process, heat input is influenced by welding current, voltage, and travel speed (Datta et al. 2002) (Saad et al. 2025). If the heat input is too low, the weld may suffer from insufficient penetration. Conversely, excessive heat input may cause thermal distortion, excessive grain growth, and a reduction in hardness (Jose and Ii, 2010) (Mahajan, 2019). Therefore, proper control of heat input is essential to ensure that the weld meets the desired mechanical and structural performance standards (Datta et al. 1998) (Mohandas et al. 1999).

Previous studies have examined the influence of welding current and voltage on the hardness and tensile strength of SS400 steel (Engineering, 1993) (Olawale et al. 2012). However, most of these studies focused solely on current variations without directly connecting the results to heat input values expressed in kJ/mm, which actually represent the total thermal energy absorbed by the material (Raja et al. 2015) (Dadi et

al. 2018). In addition, research specifically investigating the relationship between heat input, microstructural changes in the fusion zone and heat-affected zone (HAZ), and mechanical properties simultaneously remains limited (Ahmed et al. 2016) (Kchaou et al. 2014).

This study aims to evaluate how variations in heat input during SMAW affect the microstructure and mechanical properties of SS400 low-carbon steel. Three heat input levels 1.24 kJ/mm, 1.84 kJ/mm, and 2.20 kJ/mm were examined. The experimental procedures included microstructural analysis, Vickers hardness testing, and tensile tests to determine the correlation between the thermal energy supplied and the resulting weld quality. The findings of this study are expected to serve as a reference for determining the most suitable heat input parameter to improve weld quality in industrial applications involving SS400 steel (Paul, 2016) (Arifin, 2020).

Beyond process parameters, electrode type and welding technique also play vital roles in determining the quality of welded joints in SS400 steel. The selection of an appropriate electrode influences arc stability, filler metal melting rate, and heat distribution within the weld area (Haider et al. 2019). In practice, using electrodes with the proper diameter and coating type can help maintain heat input within an acceptable range (Alkahla and Pervaiz, 2017). Operator technique including electrode angle, arc length, and travel speed also contributes significantly to weld consistency, defect prevention, and mechanical performance (Weerasekralage et al. 2019).

Furthermore, understanding the correlation between heat input and material behavior is crucial in quality control of welded products. An optimal heat input can produce a fine and homogeneous microstructure, enhancing resistance to cracking and thermal deformation (Alhuzaim 2024). In contrast, imbalanced thermal energy may create excessively hard or soft zones, reducing the joint's ability to withstand dynamic loads. Thus, studies on heat input variations for SS400 steel not only contribute academically but also provide practical value by guiding industries to design efficient, economical, and safe welding parameters for structural applications (Garga et al. 2026).

Additionally, the results of this research are expected to offer a more comprehensive understanding of how welding parameters affect material performance after joining. By identifying safe limits and the effects of each heat input variation on SS400 mechanical properties, industries can implement more accurate and measurable welding standards especially for components operating under cyclic or high-temperature conditions (Omiogbemi et al. 2025). The generated data may also be used in developing predictive models of post-weld material behavior, such as thermal and mechanical simulations using finite element methods, which help reduce costly trial-and-error procedures in real industrial settings (Baghel, 2022). Moreover, insights into the interaction between thermal energy, cooling rate, and phase transformation in low-carbon steel can support engineers in determining appropriate preheating, interpass temperature, and post-weld heat treatment strategies to minimize residual stress and thermal deformation (Yu et al. 2025). Therefore, this study not only strengthens theoretical knowledge in welding

metallurgy but also contributes to the implementation of more efficient, standardized, and quality-oriented welding technology for low-carbon steel applications.

Based on previous studies (Eko, 2018), the influence of heat input on the mechanical properties of low-carbon steel has been widely discussed; however, most research focuses on macroscopic parameters such as tensile strength or hardness. Microstructural analyses in earlier studies were largely qualitative and did not explicitly correlate ferrite pearlite transformations with two key mechanical parameters: tensile strength and yield strength. Furthermore, many studies were conducted on general low-carbon steels such as AISI 1018 or mild steel, rather than specifically on SS400, which is commonly used in structural applications.

Therefore, the novelty of this research lies in its integrated approach combining heat input variations, quantitative microstructural analysis, and simultaneous evaluation of tensile strength and yield strength of SS400 steel welded using the SMAW process. This approach has been rarely explored, and the findings are expected to provide a more comprehensive understanding of how heat input affects the mechanical behavior and weld quality of SS400 low-carbon steel.

Research methods

This study was conducted to investigate the effect of varying heat input levels on the microstructure and mechanical properties of SS400 low-carbon steel welded using the SMAW process. The experimental procedures were designed to ensure consistency in welding parameters, material preparation, and testing methods so that the influence of heat input could be observed accurately. All welding experiments, specimen preparations, and mechanical tests were carried out in accordance with relevant welding and metallurgical testing standards to maintain the validity and reliability of the results.

Equipment materials

The primary material used in this study was SS400 low-carbon steel plates with a thickness of 8 mm and specimen dimensions of 300 × 100 mm. The electrode used for welding was an E7018 type with a diameter of 3.2 mm, and a 60° V-groove joint preparation was applied. The welding process was performed using a Shielded Metal Arc Welding (SMAW) machine with a direct current (DC) power source.

Welding procedure

1. Welded specimen preparation

A 60° V-groove preparation and a butt joint configuration were used for the welding specimens, as illustrated in Figure 1.

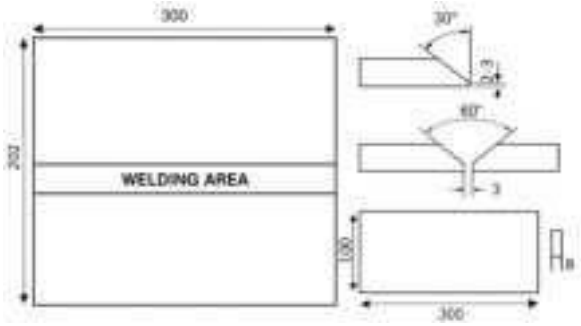


Figure 1. Welding specimen design

The specimens used in this study were SS400 low-carbon steel plates with dimensions of 300 mm × 100 mm × 8 mm. A total of six plates were prepared and welded into three paired

specimens, each using a different welding current variation. The welding process was carried out using the Shielded Metal Arc Welding (SMAW) method.

The stages of the specimen preparation and welding process were conducted as follows:

1. Preparing all required tools and materials, including SS400 steel plates.
2. Wearing appropriate personal protective equipment (PPE) according to safety procedures.
3. Cutting the material to the predetermined dimensions using a grinding machine.
4. Creating a 30° bevel on one side of each specimen using a hand grinder, then verifying the bevel angle using a protractor to ensure accuracy.
5. Preparing the welding equipment and ensuring all tools were in proper condition and compliant with Standard Operating Procedure (SOP) requirements.
6. Performing the welding process using E7018 electrodes with a diameter of 3.2 mm, applying a 60° V-groove butt joint, and using three variations of heat input: 1.24 kJ/mm, 1.84 kJ/mm, and 2.20 kJ/mm.
7. Inspecting the welded joints to ensure the absence of defects, followed by preparing the test specimens according to the corresponding testing standards.

2. *Microstructure examination*

The microstructure test specimens are shown in Figure 2, The microstructural examination was carried out through several preparation and observation stages to ensure that the metallurgical features of the welded specimens could be clearly identified.



Figure 2. Microstructure test specimen

First, the test samples were sectioned using a cutting machine to obtain pieces that were convenient for microscopic observation. The cut surfaces were then ground and cleaned to produce flat, parallel surfaces suitable for further preparation. Each specimen was subsequently mounted using resin to provide stability during grinding and polishing.

The mounted samples were progressively ground using abrasive papers with grit sizes of 100, 240, 600, 1000, 1500, 2000, and 5000 to achieve a smooth and uniform surface. This was followed by polishing with a cloth and autosol compound until a mirror-like finish was obtained. After polishing, the specimens were rinsed with water and thoroughly dried.

Etching was performed by immersing the polished surface for approximately 3 seconds in a Nital solution prepared by mixing nitric acid (HNO_3) and alcohol in a 1:4 ratio (5 mL HNO_3 and 20 mL alcohol). The etched specimens were then neutralized with alcohol, rinsed again with water, and dried completely. Finally, the etched microstructures were examined using an optical microscope, and the observed features were documented photographically for further metallurgical analysis.

The process of the microstructure test specimens are illustrated in Figure 3, which shows the polishing process and the etching process performed prior to optical microscope observation.

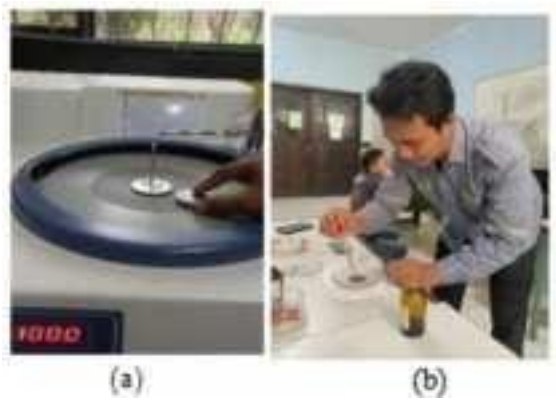


Figure 3. (a) Polishing process, (b) Etching process

3. Tensile testing

The tensile test specimens were prepared in accordance with the ASTM E8 standard in the form of flat plate specimens, as shown in Figure 4.

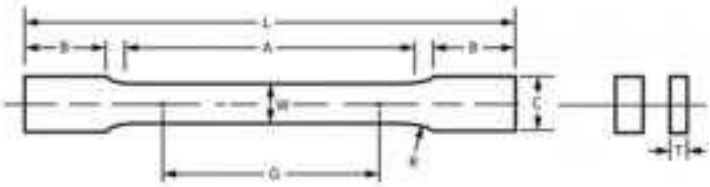


Figure 4. ASTM E8 tensile test specimen

The dimensional specifications of the tensile test specimen are shown in Figure 5. The specimen has an overall length (L) of 200 mm, a width (B) of 50 mm, and a reduced section width (C) of 20 mm. The fillet radius (R) and the gauge width (W) are both 12.5 mm. The gauge length (G) is 50 mm, the grip section length (A) is 80 mm, and the specimen thickness (T) is 8 mm. These dimensions follow the ASTM E8 requirements for flat tensile test specimens.

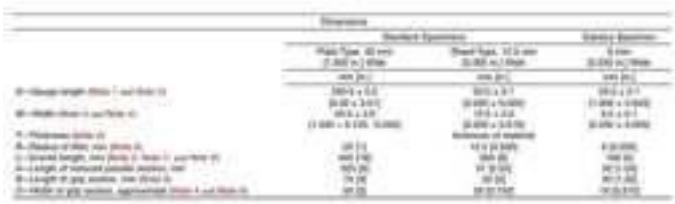


Figure 5. Source data from american society for testing and materials

The tensile test was carried out through several sequential steps. First, the test specimens were machined to meet the dimensional requirements specified in the tensile testing standard. Second, the universal testing machine was prepared and calibrated to ensure measurement accuracy. Third, after the machine was powered on, an initial warm-up and parameter setup were performed using the computer system connected to the equipment. Fourth, the specimen was mounted between the machine grips, ensuring that it was properly aligned to minimize the risk of off-axis loading. Fifth, the testing parameters such as loading rate and elongation limit were set according to the applicable standard. Sixth, the test was conducted by gradually applying tensile load until the specimen fractured or experienced complete failure. Finally, the maximum load, elongation, strain, and other relevant data were automatically recorded by the computer system for subsequent analysis.

Results and discussion

Welding Result

The heat input was calculated using the following equation:

$$Q = \left(\frac{V\ x\ I\ x\ 60}{1000xs}\right) x\ \eta (kJ/mm) \qquad \text{(Ge et al. 2024)}$$

The calculated heat input values (Q) for each welding parameter are presented in Table 1 below.

Table 1. Heat Input Calculation.

Specimen	Current	(A)Voltase	(V)Speed	(mm/minute)Heat input (Kj/mm)
1	90	24	83,91	1,24
2	110	29,25	83,91	1,84
3	130	29,6	83,91	2,2

The variables used in the heat input calculation are defined as follows: V represents the welding voltage (V), I denotes the welding current (A), S is the welding speed measured in mm/min, and η refers to the process efficiency, which is taken as 0.8 for the SMAW process. These parameters are essential for determining the total thermal energy delivered to the material during welding as shown in Table 2.

Table 2. Microstructure test results at heat input 1.24 kJ/mm

Area	Micrograph (50x)	% Ferrite	% Perlite
Base metal		51,789	48,211
Heat Affected Zone		53,472	46,528
Weld Metal		52,972	47,028

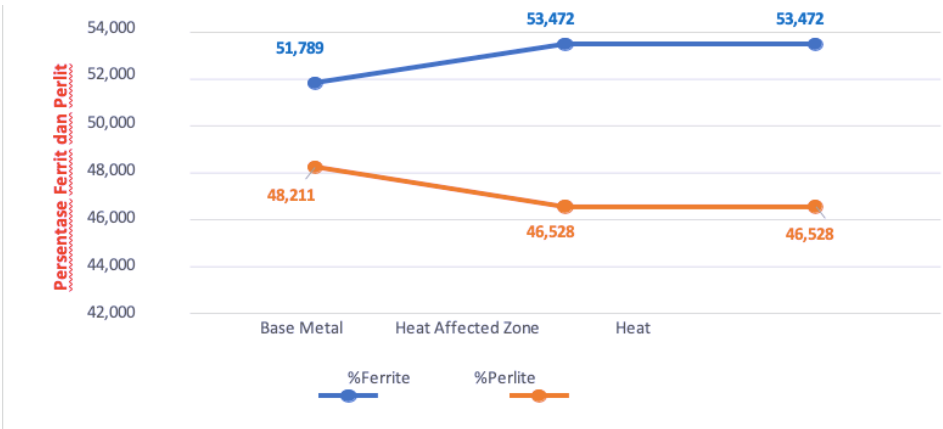


Figure 6. Relationship between ferrite and pearlite percentages in each welding region, distribution at heat input 1.24 kJ/mm

P = Pearlite, F = Ferrite, GBF = Grain Boundary Ferrite, AF = Acicular Ferrite, WF = Widmanstätten Ferrite, Figure 6 shows that in the Base Metal (BM), the ferrite content is 51.789% and the pearlite content is 48.211%. This composition aligns with the typical microstructure of low-carbon steel in its normal condition without heat treatment, indicating that the BM did not experience any phase transformation as a result of welding. Therefore, the base properties of the material remain preserved. The relatively higher pearlite content contributes to improved tensile strength and hardness, although its ductility may be slightly lower compared to regions with a higher ferrite proportion.

In the Heat Affected Zone (HAZ), the ferrite percentage increases to 53.472%, while pearlite decreases to 46.528%. This increase in ferrite and reduction in pearlite indicates

that portions of the pearlite structure have transformed due to thermal exposure during welding. This condition results in grain coarsening and a subsequent decrease in hardness within the HAZ. As a transitional region, the HAZ balances strength and toughness between the unaffected base metal and the weld metal. Hence, controlling the thermal input and cooling rate in this region is essential to maintain the mechanical reliability of the welded joint.

In the Weld Metal (WM), the ferrite content slightly decreases to 52.972%, while the pearlite content increases to 47.028%. This condition corresponds to the moderate heat input of 1.24 kJ/mm, which does not produce a cooling rate fast enough to retain a predominantly ferritic structure. The resulting microstructure consists of a mixture of acicular ferrite and fine pearlite, offering a favorable combination of hardness, strength, and toughness. Therefore, the microstructure in the WM is well-suited for welded joints that do not require extremely high hardness but still demand good toughness under dynamic loading.

The subsequent microstructural characteristics corresponding to the heat input of 1.84 kJ/mm are shown in Table 3.

Table 3. Microstructure test results at heat input 1.84 kJ/mm

Area	Micrograph (50x)	% Ferrite	% Perlite
Base metal		51,789	48,211
Heat Affected Zone		53,472	46,528
Weld Metal		52,972	47,028

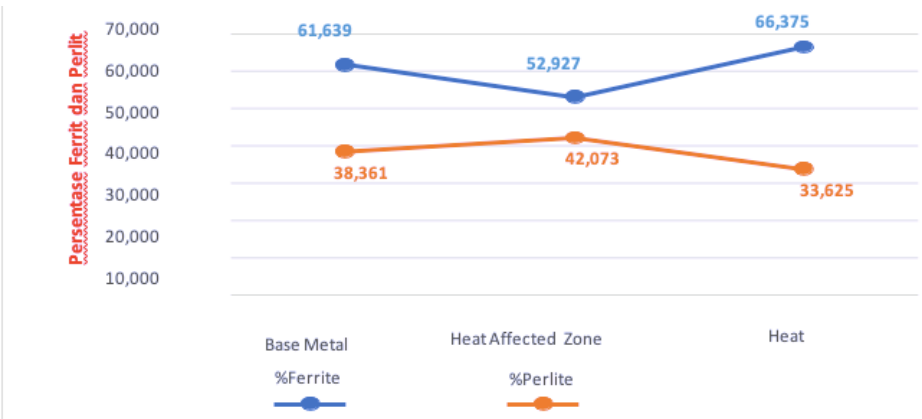


Figure 7. Relationship between ferrite and pearlite percentages in each welding region, distribution at heat input 1.84 kJ/mm

P = Pearlite, F = Ferrite, GBF = Grain Boundary Ferrite, AF = Acicular Ferrite, WF = Widmanstätten Ferrite, As seen in Figure 7, the ferrite content in the Base Metal (BM) increases to 61.639%, while pearlite decreases to 38.361%. This indicates that the BM underwent slight microstructural modification due to heat diffusion from the high heat input welding process, even though it was not directly exposed to the arc. Normally, SS400 steel has a relatively balanced ferrite–pearlite composition. However, high heat input can cause extended heat diffusion, leading to over-tempering or partial recrystallization near the HAZ boundary. According to (Qi et al., 2024), high heat input causes slower cooling rates and broader thermal diffusion, potentially altering BM microstructure. An increase in ferrite fraction may reduce hardness and tensile strength but can improve toughness.

In the HAZ, the ferrite content is 52.927%, slightly lower than in the BM, while pearlite increases to 42.073%. This suggests that although the HAZ experienced elevated temperatures, the cooling rate was still sufficient to allow partial pearlite formation. The higher pearlite content compared to WM indicates that the HAZ remains a transitional zone with mixed mechanical characteristics. Since the HAZ does not melt, its microstructural changes primarily involve partial phase transformation and grain growth. As supported by (Qi et al., 2024), high heat input reduces cooling rates, altering austenite grain size and transformation products, thereby affecting the ferrite–pearlite ratio and the presence of AF, GBF, or WF. Consequently, the HAZ retains more pearlite than the WM under high heat input.

In the Weld Metal (WM), the ferrite content increases substantially to 66.375%, while pearlite decreases to 33.625%. This is the highest ferrite content among all regions, indicating that slow cooling resulting from high heat input promotes the formation of primary ferrite and grain boundary ferrite. The slower solidification rate allows ferrite grains to grow significantly, leading to reduced hardness and tensile strength in the weld metal and creating a softer zone in the WM. Such conditions are common in welds made with high current or low travel speed. Although a high ferrite fraction improves ductility and toughness, it reduces wear resistance and tensile strength.

The subsequent microstructural characteristics corresponding to the heat input of 2.2 kJ/mm are shown in Table 4.

Table 4. Microstructure test results at heat input 2.2 kJ/mm

Area	Micrograph (50x)	% Ferrite	% Perlite
Base metal		43,946	43,946
Heat Affected Zone		43,946	43,946

Weld Metal		43,946	43,946

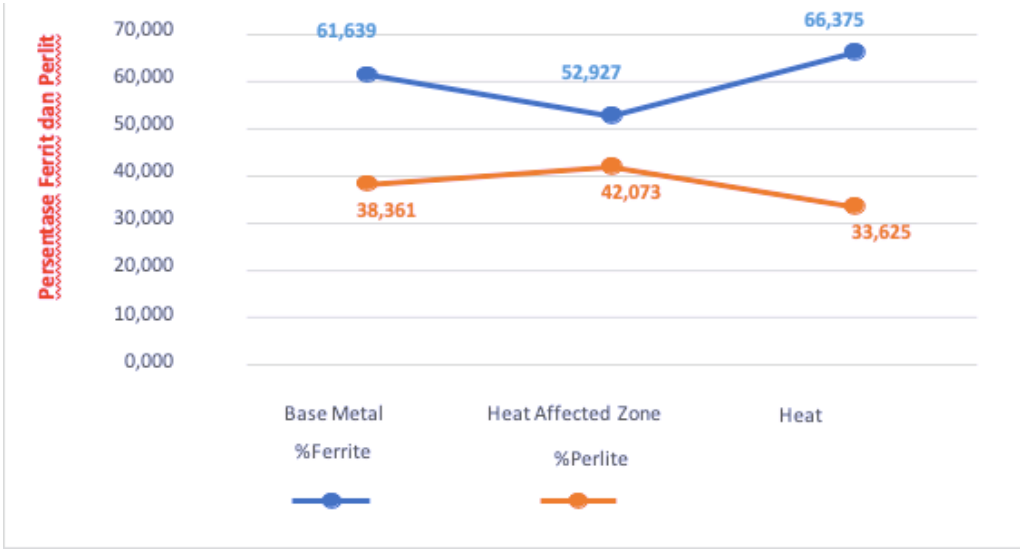


Figure 8. Relationship between ferrite and pearlite percentages in each welding region, distribution at heat input 2.2 kJ/mm

P = Pearlite, F = Ferrite, GBF = Grain Boundary Ferrite, AF = Acicular Ferrite, WF = Widmanstätten Ferrite, As seen in Figure 8 shows that in the Base Metal (BM) region, the ferrite content reaches 68.968%, indicating a predominantly ferritic structure that generally provides good ductility but only moderate strength. In the Heat Affected Zone (HAZ), the ferrite content decreases to 56.054%, indicating partial transformation of ferrite into pearlite due to the high thermal exposure during welding. This reduction is caused by the thermal cycle experienced in the HAZ, where part of the ferrite dissolves into austenite and subsequently transforms into pearlite during slow cooling.

In the Weld Metal (WM), the ferrite content increases again to 66.002%. This increase suggests that solidification in the WM occurs primarily through the formation of primary ferrite due to the relatively high heat input, followed by a slow cooling rate. The re-emergence of a dominant ferritic structure in the WM may reduce hardness and tensile strength but enhances the ductility and toughness of the welded joint.

To evaluate the statistical relationship between heat input and the resulting microstructural composition, a Pearson correlation analysis was conducted using ferrite and pearlite percentages as dependent variables. The analysis was performed using SPSS with the command:

```
CORRELATIONS
/VARIABLES=HeatInput Ferrit Perlit
/PRINT=TWOTAIL NOSIG FULL
/MISSING=PAIRWISE.
```

This test determines the strength and direction of the linear correlation between heat input and each microstructural phase. A positive Pearson coefficient indicates that an increase in heat input is associated with an increase in the corresponding phase, while a negative coefficient suggests an inverse relationship. The two-tailed significance test (p-value) is used to verify whether the observed correlations are statistically meaningful. This analysis provides quantitative evidence supporting the microstructural changes observed in the metallographic results, allowing a deeper understanding of how variations in heat input influence the proportions of ferrite and pearlite in each welding region.

Table 5. Pearson correlation table

Correlations

		Heat input variation (kJ/mm)	Ferrite percentage (%) in each zone	Percentage of pearlite (%) in each zone
Heat input variation (kJ/mm)	Pearson Correlation	1	.707*	-.764*
	Sig. (2-tailed)		.033	.017
	N	9	9	9
Ferrite percentage (%) in each zone	Pearson Correlation	.707*	1	-.970**
	Sig. (2-tailed)	.033		.000
	N	9	9	9
Percentage of pearlite (%) in each zone	Pearson Correlation	-.764*	-.970**	1
	Sig. (2-tailed)	.017	.000	
	N	9	9	9

*. Correlation is significant at the 0.05 level (2-tailed).

**. Correlation is significant at the 0.01 level (2-tailed).

Based on the results of the Pearson correlation analysis, a positive correlation was found between heat input and ferrite content, with $r = 0.707$ and $p = 0.033$ ($p < 0.05$), indicating a statistically significant relationship between heat input variation and the percentage of ferrite phase in SS400 low-carbon steel at a 95% confidence level. This result suggests that increasing the heat input during welding leads to higher ferrite formation. This phenomenon occurs because higher heat input produces a slower cooling rate, allowing primary ferrite more time to grow before pearlite transformation begins.

Conversely, the relationship between heat input and pearlite shows a strong negative correlation, with $r = -0.764$ and $p = 0.017$ ($p < 0.05$), indicating that an increase in heat input results in a decrease in pearlite content. The slower cooling associated with high heat input does not sufficiently promote the carbon diffusion required for pearlite formation, leading to a reduced pearlite fraction.

In addition, the correlation between ferrite and pearlite exhibits a very strong negative relationship ($r = -0.970$, $p < 0.001$), demonstrating that the two phases are inversely

proportional. As ferrite content increases, pearlite decreases significantly. This aligns with the typical phase balance in low-carbon steel, where ferrite growth is favored at slower cooling rates, while pearlite formation is suppressed due to insufficient carbon diffusion during weld metal solidification.

Overall, the correlation results obtained in this study support fundamental welding metallurgy theory, confirming that higher heat input significantly affects cooling characteristics and microstructural development. A slower cooling rate promotes a ferrite-dominated microstructure, which enhances ductility and toughness of the weld metal. However, the dominance of ferrite also tends to reduce hardness and tensile strength of the welded joint. These findings are consistent with those reported in (Senthilkumar et al., 2023), which concluded that increasing heat input decreases tensile strength and hardness in low-carbon steel welds, although yield strength was not considered in their analysis.

Tensile test results and discussion

Metallographic testing produced a series of microstructure images, and the proportion as well as the distribution of ferrite and pearlite for each heat input variation are summarized in the tables and subsequently presented in the graphs below.

$$\sigma \max = \frac{P\max\ (MPa)\ q}{T\ X\ W} \qquad (2)$$

$$\sigma y = \frac{PL\ \ MPa}{(T\ x\ W)} \qquad (3)$$

Table 6. Tensile Test Results of Raw Material

Spesimen	T (mm)	W (mm)	PL (KN)	P (max)	σmax (Mpa)	Yield Strenght (Mpa)
1	8	12,35	44,068	44068	446,03	321,28
2	8	12,5	45,088	45088	450,88	316,74
3	8	12,5	45,088	45088	450,88	316,74
		Average			449,26	318,25

Table 4. Tensile test results of welded specimens

Heat Input (Kj/mm)	Spesimen	T (mm)	W (mm)	PL (KN)	P (max)	σmax (Mpa)	Yield Strenght (Mpa)
	1	8	12,55	47,241	47241	470,53	320,45
1,24	2	8	12,9	47,532	47532	460,58	343,09
	3	8	12,6	47,097	47097	467,23	374,11
			Average			466,11	345,89
	1	8	12,7	47,212	47212	464,69	324,09
1,84	2	8	13	42,616	42616	409,77	270,82
	3	8	12,5	40,679	40679	406,90	269,21
			Average			427,08	288,04
	1	8	12,55	46,533	46533	463,48	316,06
2,2	2	8	12,55	27,259	27259	271,50	122,50
	3	8	12,3	51,281	51281	521,15	169,61

Figure 9 shows that after the welding process with heat input variations of 1.24, 1.84, and 2.20 kJ/mm, both tensile strength and yield strength exhibit noticeable changes compared to the raw material. The tensile strength of the raw material, which is 449.26 MPa, increases by 3.75% at a heat input of 1.24 kJ/mm. However, it decreases at heat inputs of 1.84 kJ/mm and 2.20 kJ/mm, reaching 427.08 MPa (−8.37%) and 418.71 MPa (−10.17%), respectively. Similarly, the yield strength of the raw material (318.25 MPa) increases by 8.68% at 1.24 kJ/mm but then drops significantly to 288.04 MPa (−16.73%) at 1.84 kJ/mm and to 202.72 MPa (−49.7%) at the highest heat input of 2.20 kJ/mm.

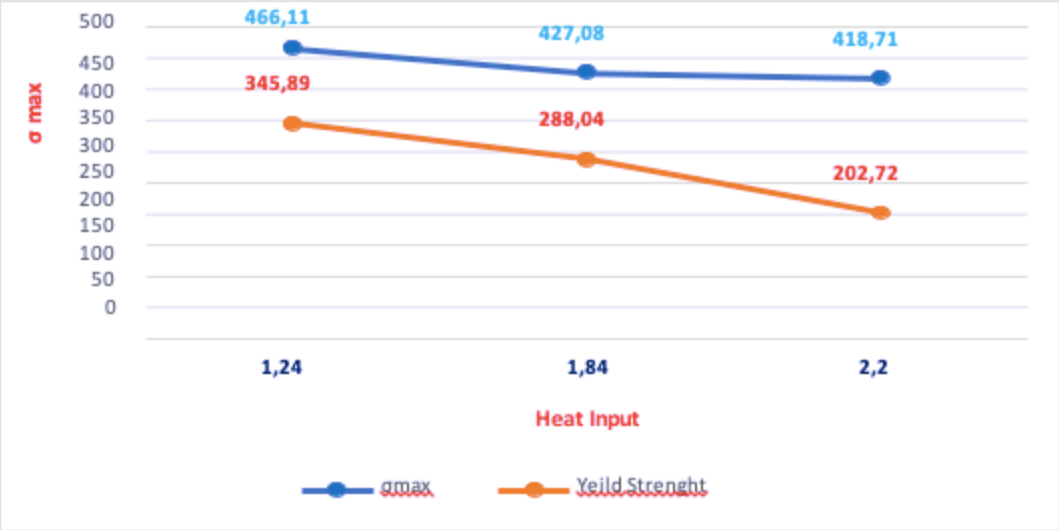


Figure 9. Comparison of tensile strength and yield strength

At the lowest heat input (1.24 kJ/mm), the welded specimen exhibits the highest tensile strength. This is attributed to the relatively faster cooling rate, which produces a finer microstructure consisting of a balanced distribution of ferrite and pearlite. Such a refined structure increases resistance to dislocation movement, thereby enhancing mechanical strength. As the heat input increases to 1.84 kJ/mm and 2.20 kJ/mm, both tensile strength and yield strength tend to decrease. Higher heat input introduces more total thermal energy into the joint, resulting in slower cooling. Slow cooling promotes grain growth and increases the proportion of ferrite, which is relatively softer, while reducing the formation of fine pearlite that contributes to strength. Consequently, the microstructure in the weld metal (WM) and heat- affected zone (HAZ) becomes coarser and less resistant to plastic deformation, leading to lower yield strength and maximum stress (σmax). These mechanical property changes are strongly influenced by microstructural modifications occurring in both WM and HAZ.

Based on the graph, a decrease of 10.17% in tensile strength and 41.39% in yield strength is observed from the lowest to the highest heat input. The higher thermal energy promotes recrystallization and grain growth during cooling, consistent with findings reported in previous studies.

Conclusion

Based on the results of this study on the effect of heat input variation in the Shielded Metal Arc Welding (SMAW) process on the mechanical properties and microstructure of SS400 low- carbon steel, the following conclusions can be drawn:

1. The variation in heat input has a significant effect on changes in the ferrite and pearlite phase proportions of SS400 low-carbon steel at a 95% confidence level.
2. Increasing the heat input from 1.24 kJ/mm to 2.20 kJ/mm leads to the growth of larger ferrite grains and a reduction in pearlite content, which weakens the mechanical strength of the material due to the reduced grain boundary area that impedes dislocation motion.
3. A heat input of 1.24 kJ/mm produces the highest mechanical performance, with a tensile strength of 466.11 MPa and a yield strength of 345.89 MPa—representing increases of 3.75% and 8.69%, respectively, compared to the raw material.
4. Increasing the heat input to 1.84 kJ/mm and 2.20 kJ/mm results in decreases in tensile strength by 0.08%–0.10% and decreases in yield strength by 16.7%–41.39%. The significant reduction in yield strength is caused by grain coarsening and a decrease in pearlite content within the weld metal and heat-affected zone (HAZ), leading to a softer material with lower hardness and higher susceptibility to plastic deformation.
5. The optimum heat input for achieving the best joint strength in SS400 steel welded using the SMAW process is 1.24 kJ/mm

References

1. Abbas, Hammada, and Ahmad Yusran Aminy. "The Effects of Shielded Metal Arc Welding (Smaw) Welding On The Mechanical Characteristics With Heating Treatment Inn S45c Steel The Effects of Shielded Metal Arc Welding (Smaw) Welding On The Mechanical Characteristics With Heating Treatment Inn S45c Steel."
2. Adi Nugroho dan Eko. 2018. "Jurnal Skirpsi 17." Pengaruh Variasi Kuat Arus Pengelasan Terhadap Kekuatan Tarik Dan Kekerasan Sambungan Las Plate Carbon Steel Astm 36 3(2): 134–42.
3. Ahmed, Ali N, C W Mohd Noor, Mohammed Falah, and Allawi Ahmed. 2016. "RBF-NN- Based Model for Prediction of Weld Bead Geometry in Shielded Metal Arc Welding (SMAW)." Neural Computing and Applications.
4. Ajenifuja, E, A P I Popoola, and O Popoola. 2025. "Journal of Advanced Joining Processes Comparative Analysis of Structural and Mechanical Properties of Duplex Stainless Steel (DSS) Weldments Prepared by Flux Core Arc Welding and Shielded Metal Arch Welding Processes." 11(February).
5. Alhuzaim, Abdullah F. 2024. "Comparative Analysis of Shielded Metal Arc Welding (SMAW) Beads in Dry and Wet Environments." 21(2): 92–96.
6. Arifin, Amir. 2020. "Dissimilar Metal Welding Using Shielded Metal Arc Welding : A Review." 62(04): 1935–48.
7. Awad, Ibrahim R, Hamed A Abdel-aleem, Ahmed Gaafer, and Mahmoud Khedr. 2025. "ScienceDirect Influence of GTAW and SMAW Techniques on the Mechanical Behavior of S275JR Low Carbon Manganese Steel Welded Joints." Procedia Structural Integrity 68: 1024–30. https://doi.org/10.1016/j.prostr.2025.06.165.
8. Baghel, Pushp Kumar. 2022. "Heliyon Effect of SMAW Process Parameters on Similar and Dissimilar

Metal Welds : An Overview." Heliyon 8(12): e12161. https://doi.org/10.1016/j.heliyon.2022.e12161.
9. Dadi, Afnan, Proff Bhupesh Goyal, and Hardik Patel. 2018. "A Review Paper o n " Optimization of Shielded Metal Arc Welding Parameters for Welding of (Ms) Sa-516 Gr . 70 Plate by Using Taguchi Approach." 4(5): 1536–43.
10. Datta, R et al. 2002. "Weldability Characteristics of Shielded Metal Arc Welded High Strength Quenched and Tempered Plates." 11(February): 5–10.
11. Datta, R, D Mukerjee, and S Mishra. 1998. "Weldability and Toughness Evaluation of Pressure Vessel Quality Steel Using the Shielded Metal Arc Welding (SMAW) Process. 7(December): 817–23.
12. Engineering, Knowledge. 1993. "Knowledge Engineering A Shielded Metal Arc Welding Expert System." 21: 121–29.
13. Garga, Abhinav, Sanjeev Kumar, and Chandan Pandey. 2026. "Comparative Assessment of Ni-Based Electrodes on the Integrity of Inconel 617-AISI 304 H Dissimilar Welds for Advanced Ultra-Supercritical Boilers." Materials Today Communications 50(September 2025): 114254. https://doi.org/10.1016/j.mtcomm.2025.114254.
14. Ge, Guangnan et al. 2024. "Effect of Heat Input on the Microstructure and Performance of Dissimilar Welded Joint between Q345B Low-Alloy Steel and 2205 Duplex Stainless Steel." Journal of Materials Research and Technology 33(October): 4858–74. https://doi.org/10.1016/j.jmrt.2024.10.165.
15. Haider, S Farrukh et al. 2019. "Effect of Shielded Metal Arc Welding (SMAW) Parame- Ters on Mechanical Properties of Low-Carbon , Mild and Stainless-Steel Welded Joints : A Review." 5(5): 191–98.
16. Jose, Eduardo, and Lima Ii. 2010. "Robotic Shielded Metal Arc Welding." 89(August). Kchaou, Y et al. 2014. "Microstructural , Compositional and Mechanical Investigation of
17. Shielded Metal Arc Welding (SMAW) Welded Superaustenitic UNS N08028 (Alloy 28) Stainless Steel." JOURNAL OF MATERIALS&DESIGN 63: 278–85. http://dx.doi.org/10.1016/j.matdes.2014.06.014.
18. Mahajan, Sumit. 2019. "Design and Development of Shielded Metal Arc Welding (SMAW) Electrode Coatings Using a CaO-CaF 2 -SiO 2 and CaO-."
19. Mohandas, T, G Madhusudhan Reddy, and Mohammad Naveed. 1999. "A Comparative Evaluation of Gas Tungsten and Shielded Metal Arc Welds of a `` Ferritic ' ' Stainless Steel." 94: 133–40.
20. Muthusamy, Chellappan et al. 2016. "Effect of Heat Input on Mechanical and Metallurgical Properties of Gas Tungsten Arc Welded Lean Super Martensitic Stainless Steel 2 . EXPERIMENTAL PROCEDURE :" 19(3): 572–79.
21. Olawale, J O et al. 2012. "Correlation between Process Variables in Shielded Metal-Arc Welding (SMAW) Process and Post Weld Heat Treatment (PWHT) on Some Mechanical Properties of Low Carbon Steel Welds." 2012(September): 891–95.
22. Omiogbemi, Ibrahim Momoh-bello et al. 2025. "Influence of SMAW and GMAW on Mechanical , Microstructural , and Corrosion Properties of High-Carbon Steel." Next Research 2(4): 101026. https://doi.org/10.1016/j.nexres.2025.101026.
23. Pagare, Rohit, and Dhanesh Awati. "Sustainability Assessment of Shielded Metal Arc Welding (SMAW) Process Sustainability Assessment of Shielded Metal Arc Welding (SMAW) Process."
24. Paul, Arun Kumar. 2016. "Robust Product Design Using SOSM for Control of Shielded Metal Arc Welding (SMAW) Process." 0046(IC).
25. Qi, Huan, Qihang Pang, Weijuan Li, and Shouyuan Bian. 2024. "Effect of High Welding Heat Input on the Microstructure and Low - Temperature Toughness of Heat Affected Zone in Magnesium - Treated EH36 Steel." Scientific Reports: 1–12. https://doi.org/10.1038/s41598-024-70562-9.
26. Saad, Muhammad et al. 2025. "Optimization of Process Parameters for Shielded Metal Arc Welding for ASTM A 572 Grade 50." Journal of Engineering Research 13(2): 1072–88. https://doi.org/10.1016/j.jer.2024.01.005.
27. Alkahla, Ibrahim and Pervaiz, Salman. 2017. "Sustainability Assessment of Shielded Metal Arc Welding (SMAW) Process Sustainability Assessment of Shielded Metal Arc Welding (SMAW) Process.", IOP Conference Series: Material Science and Engineering. 244 (1). https://doi.org/10.1088/1757-899X/244/1/012001
28. Taylor, Publisher et al. "Journal of Occupational and Environmental Hygiene." (June 2014): 37–41.
29. Vimal, K E K, S Vinodh, and A Raja. 2015. "Modelling , Assessment and Deployment of Strategies for Ensuring Sustainable Shielded Metal Arc Welding Process e a Case Study." Journal of Cleaner Production. http://dx.doi.org/10.1016/j.jclepro.2015.01.049.
30. Weerasekralage, L S Sisira K, M Karunarathne, and S D Pathirana. 2019. "Optimization of Shielded Metal Arc Welding (SMAW) Process for Mild Steel Optimization of Shielded Metal Arc Welding (

SMAW) Process for Mild Steel." (October).
31. Xia, Chunzhi, and Sindo Kou. 2021. "Calculating the Susceptibility of Carbon Steels to Solidification Cracking During Welding." Metallurgical and Materials Transactions B 52(1): 460–69. https://doi.org/10.1007/s11663-020-02021-5.
32. Yu, Chenjun et al. 2025. "Materials Characterization Characterization of Carbides in Nickel- Base Weld Metals of 13 % Ni Steel and First-Principles Study of Their Hydrogen Solubility." *Materials Characterization* 229(PB): 115625. https://doi.org/10.1016/j.matchar.2025.1156